JCTC Journal of Chemical Theory and Computation

ARTICLE

pubs.acs.org/JCTC

Energy-Specific Linear Response TDHF/TDDFT for Calculating High-Energy Excited States

Wenkel Liang,[†] Sean A. Fischer,[†] Michael J. Frisch,[‡] and Xiaosong Li*[,†]

[†]Department of Chemistry, University of Washington, Seattle, Washington, United States 98195

[‡]Gaussian, Inc., 340 Quinnipiac St Bldg 40, Wallingford, Connecticut 06492, United States

ABSTRACT: An energy-specific TDHF/TDDFT method is introduced in this article for excited state calculations. This approach extends the conventional TDHF/TDDFT implementation to obtain excited states above a predefined energy threshold. The method introduced and developed in this work enables computationally efficient yet rigorous calculations of energy-specific spectra, e.g., X-ray absorption involving extremely high-energy transitions. All transitions are solved in the full molecular orbital space, and orthogonality to the ground state and lower-lying excited states is preserved for each high-energy excited state. Encouraging computational savings are observed in calculating the targeted energy spectrum, while the transition energies, as well as oscillator strengths, remain identical to the results from the standard implementation.

I. INTRODUCTION

Single-reference methods such as configuration interaction singles (CIS)[1] and the linear-response variants of time-dependent Hartree−Fock (TDHF)[2,3] and time-dependent density functional theory (TDDFT)[4−7] are widely used for *ab initio* calculations of electronic excited states for large molecular systems because of their balance of computational efficiency and accuracy for practical applications.[8−11] Highly correlated methods, such as symmetry adapted cluster/configuration interaction (SAC−CI[12]), linear response coupled cluster (LRCC[13]), and equation-of-motion coupled cluster (EOM-CC[14,15]) and multireference approaches, such as multireference configuration interaction (MRCI[16]) and multireference perturbation theories (MRMP[17] and CASPT2[18]) are capable of providing more accurate treatments of excited states, including those with multielectron excitation character. However, these methods are generally computationally prohibitive for large molecules.

Conventional TDHF and TDDFT are subject to some nontrivial problems. For example, excitation energies for Rydberg and charge transfer states are often underestimated. The latter can be improved with the range-separated class of hybrid DFT functionals.[19−22] Neither TDHF nor TDDFT properly include the effects of dispersion. However, efforts have been made to include dispersion in DFT functionals, and promising results have been obtained.[23−25] The lack of correlation, or approximate nature of the treatment thereof, in standard implementations of TDHF and TDDFT results in the methods being unable to correctly describe excited states with multielectron excitation character.[26,27] In spite of these limitations, the TDHF and TDDFT methods can generally be expected to reproduce trends for one-electron valence excitations, which contribute to a majority of transitions of photochemical interest. TDDFT using hybrid density functionals, in particular, has been successful in modeling the optical absorption spectra of large molecules.[28] Recent studies have further extended the application of TDDFT to predict very high-energy, core−electron excitations that account for the pre-edge features in X-ray absorption spectroscopy (XAS).[29−31] A simple frozen-orbital method has been proposed and found to be very effective in obtaining core orbital excitations.[32−35]

Although linear-response TDHF and TDDFT are among the most tractable methods for excited state calculations, they can still be computationally demanding for large molecular systems of photochemical interest. The numerical cost of solving the TDHF/TDDFT equations using iterative techniques formally scales as $O(MN^4)$, where N is the total number of basis functions and M is the number of excited states sought. With development of effective Krylov subspace algorithms and linear-scaling methods for direct Fock/Kohn−Sham operator builders, conventional implementations of the computational scaling of linear-response TDHF and TDDFT equations can be reduced to $O(MN^2) - O(MN^3)$ in complexity. Detailed studies on the numerical algorithms for solving the TDHF/TDDFT equations are available in refs 36 and 37. Notably, if many states are to be obtained simultaneously, efficiency degrades considerably as a result of increased memory and I/O requirements. For large-scale systems, the computational bottleneck of orbital transformation can be avoided by using "orbital-free" approaches.[38,39]

In cases where a certain high-energy excited state is the subject of interest, it is possible to obtain an approximate solution of the linear-response equation of TDHF/TDDFT only in the small energy-range of interest. Along those lines, Kauczor et al.[37] have demonstrated that the optimal algorithm for solving the standard and damped complex response equation[40,41] is the preconditioned iterative subspace algorithm with symmetrized trial vectors, and the use of complex damping allows for the determination of higher excited states without knowledge of lower state solutions. Tretiak et al.[36] proposed using a symmetric Wilkinson shift[42] to acquire higher-energy excited states when solving the TDHF/TDDFT equations in an orbital-independent formulation. A response function using only a subset (e.g., core orbitals) of the molecular orbitals has also been developed to reduce the

Received: July 11, 2011
Published: September 26, 2011

cost of excited state calculations using TDHF/TDDFT. For example, the frozen-orbital method truncates the molecular orbital (MO) space and considers only the transitions between core and valence orbitals.[32,33] These methods are efficient in obtaining approximate energies and electronic characteristics of high-energy excited states; however, the application is limited to core orbitals with restricted radial extent that are nearly orthogonal to all other occupied orbitals and excited states. When such orthogonality is not well preserved, calculated excited states with incomplete orbital space can lead to inaccurate oscillator strengths and unphysical electron distributions.

In this article, we introduce an energy-specific TDHF/TDDFT (ES-TD) approach to selectively calculate absorption spectra above a predefined energy threshold while maintaining the orthogonality between excited states and the ground state. The algorithm introduced herein is rigorous because the solutions are exact in the full molecular orbital space. It is based on a simple yet effective idea to bracket high-energy spectra using a Davidson-like iterative algorithm[43,44] of the spin-unrestricted TDHF/TDDFT implementation.[9] Computational performance and accuracy are compared for Rydberg excited states of an alanine dimer, ligand-to-metal charge transfer transitions in Mn^{2+}-doped ZnO semiconductor nanocrystals, and high-energy X-ray absorptions in a set of metal tetrachlorides.

II. METHODOLOGY

In conventional linear-response TDHF/TDDFT theory, excitation energies ω can be determined by solving the non-Hermitian eigenvalue equation, given in matrix form as[6,8,9]

$$\begin{pmatrix} \mathbf{A} & \mathbf{B} \\ \mathbf{B} & \mathbf{A} \end{pmatrix} \begin{pmatrix} \mathbf{X} \\ \mathbf{Y} \end{pmatrix} = \omega \begin{pmatrix} 1 & 0 \\ 0 & -1 \end{pmatrix} \begin{pmatrix} \mathbf{X} \\ \mathbf{Y} \end{pmatrix} \tag{1}$$

with the matrices for TDHF

$$\begin{aligned} A_{ia,jb} &= \delta_{ij}\delta_{ab}(\varepsilon_a - \varepsilon_i) + (ia|jb) - (ib|ja) \\ B_{ia,jb} &= (ia|bj) - (ij|ba) \end{aligned} \tag{2}$$

and for TDDFT

$$\begin{aligned} A_{ia,jb} &= \delta_{ij}\delta_{ab}(\varepsilon_a - \varepsilon_i) + (ia|jb) - \alpha(ib|ja) + (ia|f_{xc}|jb) \\ B_{ia,jb} &= (ia|bj) - \alpha(ij|ba) + (ia|f_{xc}|bj) \end{aligned} \tag{3}$$

where $\mathbf{X}$ and $\mathbf{Y}$ are the first order electron density responses determined by solving this system of linear equations. The regular two-electron integrals are expressed in Mulliken notation. For hybrid DFT, the HF exchange integral takes on a fractional value scaled by a nonzero scaling factor α, while $\alpha = 0$ for pure DFT kernels. The response of the exchange-correlation (xc) potential term, also called the xc kernel, is given as

$$(ia|f_{xc}|jb) = \int\int \phi_i^*(r)\,\phi_a(r)\,\frac{\delta^2 E_{xc}}{\delta\rho(r)\,\delta\rho(r')}\,\phi_j^*(r')\,\phi_b(r')\,dr\,dr' \tag{4}$$

The i and j and the a and b indices represent occupied and virtual molecular orbitals (MOs), respectively, in the HF/Kohn−Sham ground state configuration.

For real orbitals, eq 1 can be reduced to a non-Hermitian (eq 5) or Hermitian (eq 6) eigenvalue equation with half the dimension

$$(\mathbf{A} - \mathbf{B})(\mathbf{A} + \mathbf{B})|\mathbf{X} + \mathbf{Y}\rangle = \omega^2|\mathbf{X} + \mathbf{Y}\rangle \tag{5}$$

$$(\mathbf{A} - \mathbf{B})^{1/2}(\mathbf{A} + \mathbf{B})(\mathbf{A} - \mathbf{B})^{1/2}\mathbf{T} = \omega^2\mathbf{T} \tag{6}$$

$$\mathbf{T} = (\mathbf{A} - \mathbf{B})^{-1/2}(\mathbf{X} + \mathbf{Y}) \tag{7}$$

If all solutions of these equations are sought, $\mathbf{A}$ and $\mathbf{B}$ include all transitions between occupied and unoccupied molecular orbitals. The size of $\mathbf{A}$ and $\mathbf{B}$ in the molecular orbital space is $(N_{occ} \times N_{unocc})^2$ where N_{occ} and N_{unocc} are the numbers of occupied and unoccupied molecular orbitals. Such a full treatment has a significantly large computational cost. An efficient algorithm to solve the response equation of TDHF/TDDFT was introduced by Stratmann et al. based on the nonsymmetric Davidson diagonalization algorithms of Hirao and Nakatsuji[44] and Bouman et al.[45] for obtaining lower-lying excited states.[9] The idea is to solve the response function in the reduced form of eq 5 or 6. The solutions can be obtained by a symmetric diagonalization or Davidson's algorithm.[43,44] In this work, we introduce additional algorithms to bracket trial vectors and eigenvalues in the predefined energy range to eventually obtain high-energy excitation energies and transitions without the effort of scanning through lower-lying excited states. We choose the Stratmann method[9] as the basic equation solver integrated with an energy screening and bracketing idea. For simplicity, we will only present the algorithm within the framework of the Hermitian eigenvalue equation (eq 6). The non-Hermitian version of the method can be readily obtained with simple matrix transformations.

The following discussions assume that M excited states with energies greater than ω_0 are the subject of interest. The $(\mathbf{A} + \mathbf{B})$ and $(\mathbf{A} - \mathbf{B})$ matrices in eq 6 are first projected onto a subspace spanned by a set of zeroth order trial vectors $\mathbf{C} = \{\mathbf{b}_1, ..., \mathbf{b}_l\}$ where $l > M$

$$\tilde{\mathbf{M}}^+ = \mathbf{C}^{\mathrm{T}}(\mathbf{A} + \mathbf{B})\mathbf{C} \tag{8}$$

$$\tilde{\mathbf{M}}^- = \mathbf{C}^{\mathrm{T}}(\mathbf{A} - \mathbf{B})\mathbf{C} \tag{9}$$

$$\tilde{\mathbf{M}} = (\tilde{\mathbf{M}}^-)^{1/2}(\tilde{\mathbf{M}}^+)(\tilde{\mathbf{M}}^-)^{1/2} \tag{10}$$

where the dimension of the resulting matrices is l. Because the number of trial vectors l is much smaller than $N_{occ} \times N_{unocc}$, the computational cost of directly generating the resulting matrices in eq 6 is greatly reduced. On the other hand, the initial l needs to be much larger than the requested number of excited states to include all MO transition candidates that may contribute significantly to excitations in the desired energy range. In the current implementation, we construct initial trial vectors by sampling the Koopmans' MO transitions for the requested energy range. $l = 4M$ trial vectors are generated in the first step, corresponding to the lowest energy Koopmans' transitions with a constraint of

$$\varepsilon_a - \varepsilon_i \geq \omega_0 + \delta\omega \tag{11}$$

The $\delta\omega$ energy shift is used to approximate corrections for the errors in Koopmans' transitions for a better selection of initial trial vectors. Note that a good selection of initial trial vectors is important for a fast convergence but generally does not affect the quality of the final results because vectors that are found to

Table 1. Comparison of Select Rydberg States of an Alanine Dimer Computed Using the Regular TDHF, ES-TDHF, and a Subset Space with Removal of HOMO TDHF Methods with the aug-cc-pvdz Basis Set

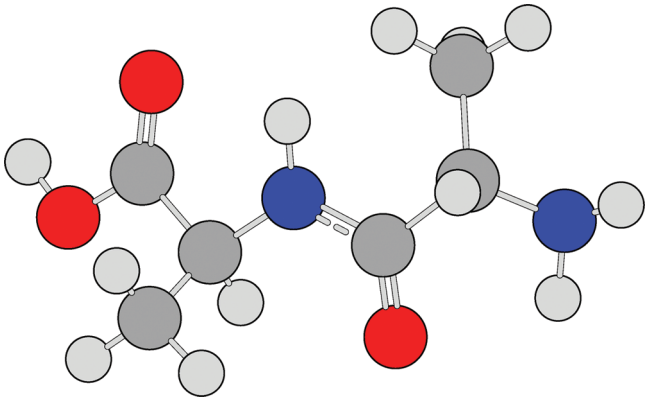

regular TDHF		ES-TDHF		subset TDHF	
excitation energy (eV)	oscillator strength (a.u.)	excitation energy (eV)	oscillator strength (a.u.)	excitation energy (eV)	oscillator strength (a.u.)
8.0767	0.1048	8.0767	0.1048	8.3037	0.0656
8.4052	0.0647	8.4052	0.0647	8.8951	0.0848
8.6152	0.0280	8.6152	0.0280	9.0088	0.0298
9.0680	0.0061	9.0680	0.0061	9.1274	0.0085
9.1148	0.0469	9.1148	0.0469	9.2649	0.0739

contribute to the excitations will be added into subspace **C** during later iterations until the convergence is achieved.

Once the reduced subspace is constructed, diagonalization of $\tilde{\mathbf{M}}$ generates a set of eigenvalues $\tilde{\omega}$ and eigenvectors $\tilde{\mathbf{T}}$ in the reduced space. In the reduced space, qualified eigenvalues and eigenvectors are selected according to the predefined requirement for excitation energy and number of excited states:

$$\tilde{\omega}_i \geq \omega_0, i = n...(n + M) \tag{12}$$

where $\tilde{\omega}_n$ is the lowest eigenvalue that is greater than the energy threshold ω_0. We define eigenvalues and eigenvectors that satisfy eq 12 as the qualified candidates in the reduced space, denoted as $\tilde{\omega}_M$ and $\tilde{\mathbf{T}}_M$. The corresponding collective transition densities, $(\tilde{\mathbf{X}} + \tilde{\mathbf{Y}})_M$ and $(\tilde{\mathbf{X}} - \tilde{\mathbf{Y}})_M$, can be obtained as well. These candidates can be transformed from the reduced space to the full MO space,

$$(\mathbf{X}' + \mathbf{Y}')_M = \mathbf{C}(\tilde{\mathbf{X}} + \tilde{\mathbf{Y}})_M \tag{13}$$

$$(\mathbf{X}' - \mathbf{Y}')_M = \mathbf{C}(\tilde{\mathbf{X}} - \tilde{\mathbf{Y}})_M \tag{14}$$

$$\omega_M' = \tilde{\omega}_M \tag{15}$$

where the primed notation refers to approximate solutions in the complete MO space. In order to estimate the errors associated with the approximate solutions, residual vectors can be defined as (see ref 9 for detailed discussions)

$$\mathbf{W}_M^L = (\mathbf{A} + \mathbf{B})(\mathbf{X}' + \mathbf{Y}')_M - \omega_M'(\mathbf{X}' - \mathbf{Y}')_M \tag{16}$$

$$\mathbf{W}_M^R = (\mathbf{A} - \mathbf{B})(\mathbf{X}' - \mathbf{Y}')_M - \omega_M'(\mathbf{X}' + \mathbf{Y}')_M \tag{17}$$

When the norm of a residual vector is below a certain small threshold (10^{-6} au in this work), the associated excited state is considered converged. For those unconverged excited states, a new set of vectors can be constructed following the Davidson algorithm:

$$\mathbf{Q}_M^L = (\omega_M' - \Delta\varepsilon)^{-1}\mathbf{W}_M^L \tag{18}$$

$$\mathbf{Q}_M^R = (\omega_M' - \Delta\varepsilon)^{-1}\mathbf{W}_M^R \tag{19}$$

where the $\Delta\varepsilon$ is the orbital energy difference. These new vectors will be orthonormalized and added into the subspace **C**, and new iteration starts from eq 8 until all vectors are converged. Note that a monotonic convergence of the reduced eigenspace can be observed because MacDonald's theorem[46] applies when the reduced subspace is unchanged.[9] Usually after a few initial iterations, the subspace of interest becomes well-defined and remains the same. A monotonic convergence can then be observed.

The algorithm introduced above is a simple extension with subspace bracketing and energy spectrum selection to the Stratmann method based on the Davidson algorithm. It is worth noting that because linear transformations are always carried out of (**A**+**B**) and (**A**−**B**) matrices, symmetrized trial vectors are introduced in each iteration, which gives optimal efficiency for standard response equation as suggested by Kauczor et al.[37] This approach is different from other approximate methods[34,35] that make use of an incomplete MO space and neglect contributions from other minor transitions. Note that the reduced subspace is used merely for the sake of obtaining solutions that correspond to a desired energy range at low computational cost. The convergence is verified in the full MO space. The size of the reduced subspace expands during iterations to include all significant transition pairs. The final results are true eigenvalues and eigenvectors of the linear-response TDHF/TDDFT equations. The resulting

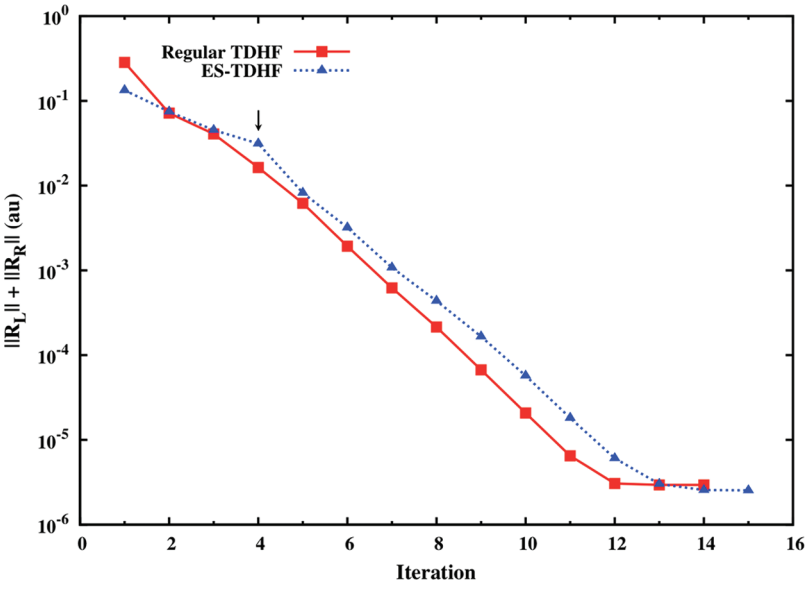

Figure 1. Convergence performance of the regular TDHF and the ES-TDHF methods for the first Rydberg state of alanine dimer. Residual norm is plotted against iteration number in the Davidson algorithm. The arrow indicates when the selected subspace starts to become stable and remain constant.

high-energy excited states are intrinsically orthogonal to lower lying states because eigenvectors in the full space corresponding to different eigenvalues are automatically biorthogonal. Numerical tests in the next section will show that not only can this method directly and accurately obtain high-energy excited states without scanning through lower-lying ones, the calculated excited states also maintain orthogonality to the ground state and to lower-lying states that are skipped in the calculations.

III. BENCHMARKS AND DISCUSSION

Calculations were carried out on a Dell PowerEdge R610 Server (dual quad-core 2.4 GHz Intel Xeon with 16 GB of RAM), using the development version of the Gaussian series of programs[47] with the addition of energy-specific linear-response TDHF/TDDFT approach presented here. The computational time reported in this article is the absolute total CPU time. In the next two sections, we will test the ES method on the Rydberg states of an alanine dimer, charge transfer excitation in a 1.0 nm quantum dot doped with a transition metal, and X-ray absorption spectra of a series of metal tetrachlorides.

A. Rydberg States of Alanine Dimer. Rydberg states of a molecule are generally associated with characteristics of high excitation energies and diffusive electronic distributions. Calculations of Rydberg states usually require large basis sets with diffusive functions, and the transition vectors of these states strongly depend on many orbitals. As a result, the excited states are very sensitive to the quality of calculations. This can be considered a stringent test case for the ES method developed herein. Table 1 lists the excitation energies and oscillator strengths of select Rydberg states of an alanine dimer molecule computed at the TDHF/aug-cc-pvdz level of theory. The first excited state lies ~6.6 eV above ground state. An energy threshold of 8 eV is used in the ES-TDHF method, which skips three lower energy valence states. The results from the first two different calculations using the regular approach and the ES-TDHF method are essentially identical. Residual norms of eqs 16 and 17 are plotted against iteration number in the Davidson algorithm in Figure 1. The convergence performance of the two methods are very similar for the first Rydberg state, though ES-TDHF may take a few more iterations to reach final convergence due to smaller initial expansion vector space. Most importantly, both methods exhibit a monotonic convergence. Such behavior has been shown mathematically in a recent work by Kauczor et al.[37] The transition vectors are also in perfect agreement (errors $<10^{-5}$) in both magnitude and sign with those obtained from the regular TDHF calculation. This agreement suggests that even though lower-energy valence states were skipped in the ES-TDHF method, the resulting high-energy Rydberg states properly maintain orthogonality to the lower ones. In Table 1, we also included results from calculations using only a subset of occupied orbitals by forbidding transitions from the highest occupied orbital. Using such a frozen-orbital approach with TDHF, the calculated Rydberg type transition energies and oscillator strengths significantly deviate from the reference values. Such deviations are a result of neglecting the strong couplings between active and frozen orbitals and the inability to preserve the orthogonality to lower-lying excited states.

B. L_{VB}MCT Transitions in Semiconductor Nanocrystals. In our recent studies[48,49] of Co^{2+}- and Mn^{2+}-doped ZnO semiconductor nanocrystals, two types of charge transfer (CT) transitions were characterized by TDDFT: metal-to-ligand CT as the promotion of a transition metal (TM) dopant d electron to the ZnO conduction band ($ML_{CB}CT$) and ligand-to-metal CT as the promotion of a ZnO valence band electron to a vacant transition metal dopant d orbital ($L_{VB}MCT$). On the basis of theoretical calculation and experimental observations,[49−51] the $L_{VB}MCT$ transitions are always higher in energy than the $ML_{CB}CT$ ones in ZnO nanocrystals. The $L_{VB}MCT$ transition is at ~6.0 eV for the $Zn_{32}TMO_{33}$ nanocrystal of ~1.0 nm diameter, while the $ML_{CB}CT$ transitions take place above ~1.75 eV.[52] For detailed discussions about the characteristic transitions in a diluted magnetic semiconductor, we refer readers to our recent work using linear response TDDFT.[49]

Doped nanocrystal structures were constructed on the basis of the scheme described in ref 48, and the ground state electronic

Table 2. Comparison of Computational Costs for Obtaining L_{VB}MCT Transitions in Mn^{2+}- and Co^{2+}-Doped ZnO Nanocrystals[a]

		regular TDDFT			ES-TDDFT		
nanocrystal systems	total number of AO	total states (range in eV)	size of subspace	CPU time in h	total states (range in eV)	size of subspace	CPU time in h
$Zn_{32}CoO_{33}$	1015	120 (0.89−6.43)	1580	331.2 (1.0)	20 (6.11−6.23)	594	99.4 (0.30)
$Zn_{32}MnO_{33}$	1015	120 (3.73−6.45)	1526	319.0 (1.0)	20 (6.21−6.35)	576	92.5 (0.29)

[a] The computational cost is evaluated using the total CPU time of the regular TDDFT method as the unit reference. Note that the wall clock time is one eighth of the total CPU time.

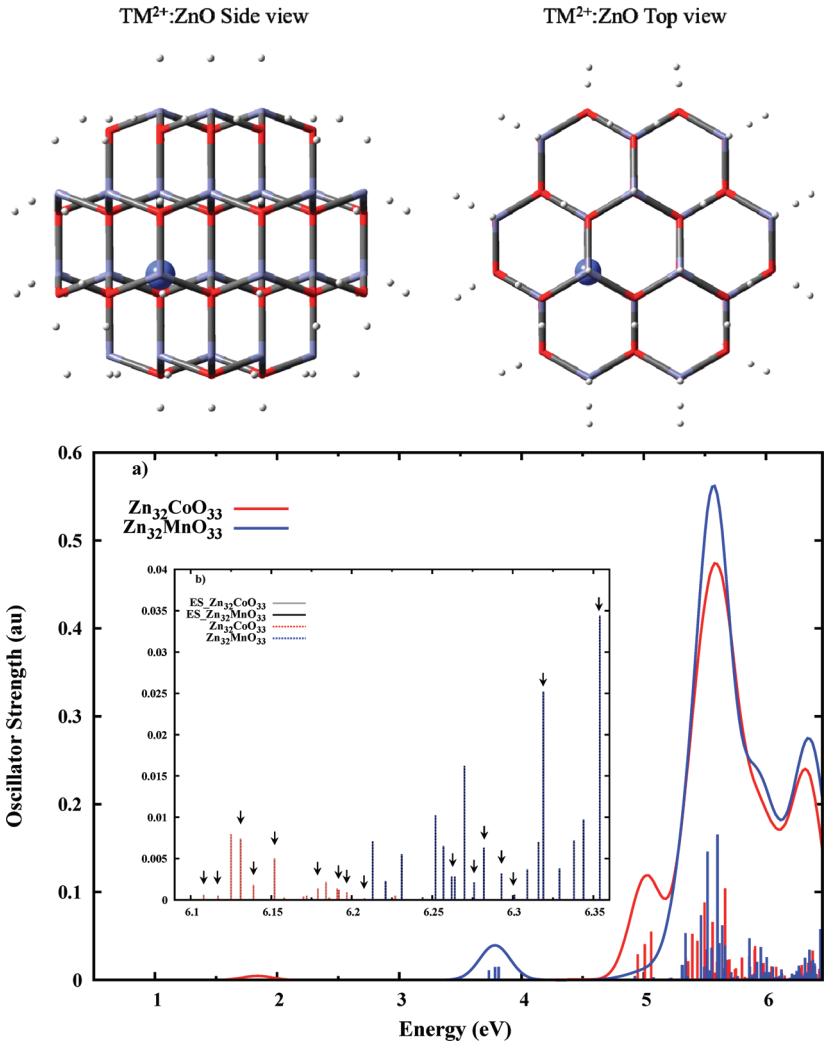

Figure 2. Top panel: Structure of the $Zn_{32}TMO_{33}H^*_{60}$ nanocrystal. The TM^{2+} dopant ion is placed close to the center of the nanocrystal and is shown as a ball. Bottom panel: Comparison of optical transition oscillator strengths calculated for Mn- and Co-doped ZnO nanocrystals with (a) regular TDDFT method and (b) ES-TDDFT approach for higher energy L_{VB}MCT transitions. TDDFT peaks are dressed with Gaussian functions and a broadening parameter of 0.12 eV. Inset shows spectrum peaks in the high excitation energy region with L_{VB}MCT transitions identified with arrows.

structures and TDDFT spectra were obtained at the PBE1PBE[53,54]/LANL2DZ[55−58] level of theory. In order to characterize the L_{VB}MCT band in the absorption spectrum, a conventional linear response TDDFT approach would need to generate as many as 120 states to be able to reach the >6.0 eV energy range. The ES-TDDFT method introduced herein can skip the lower lying excited states if a target excitation energy range is defined. Table 2 lists the computational costs of obtaining L_{VB}MCT transitions in Mn^{2+} and Co^{2+}-doped ZnO nanocrystals with both the standard implementation and the ES-TDDFT approach. The energy threshold in ES-TDDFT is set to be 6.0 eV for the $Zn_{32}TMO_{33}$ quantum dots. As shown in Figure 2, the modified algorithm yields excitation energies and oscillator strengths that are nearly identical to those obtained with the standard algorithm, with less than 1×10^{-4} eV numerical difference. The method also exhibits encouraging performance (~30% the cost of the regular calculation), even though the higher-energy transitions require more transition vectors, covering a much larger expansion vector space.

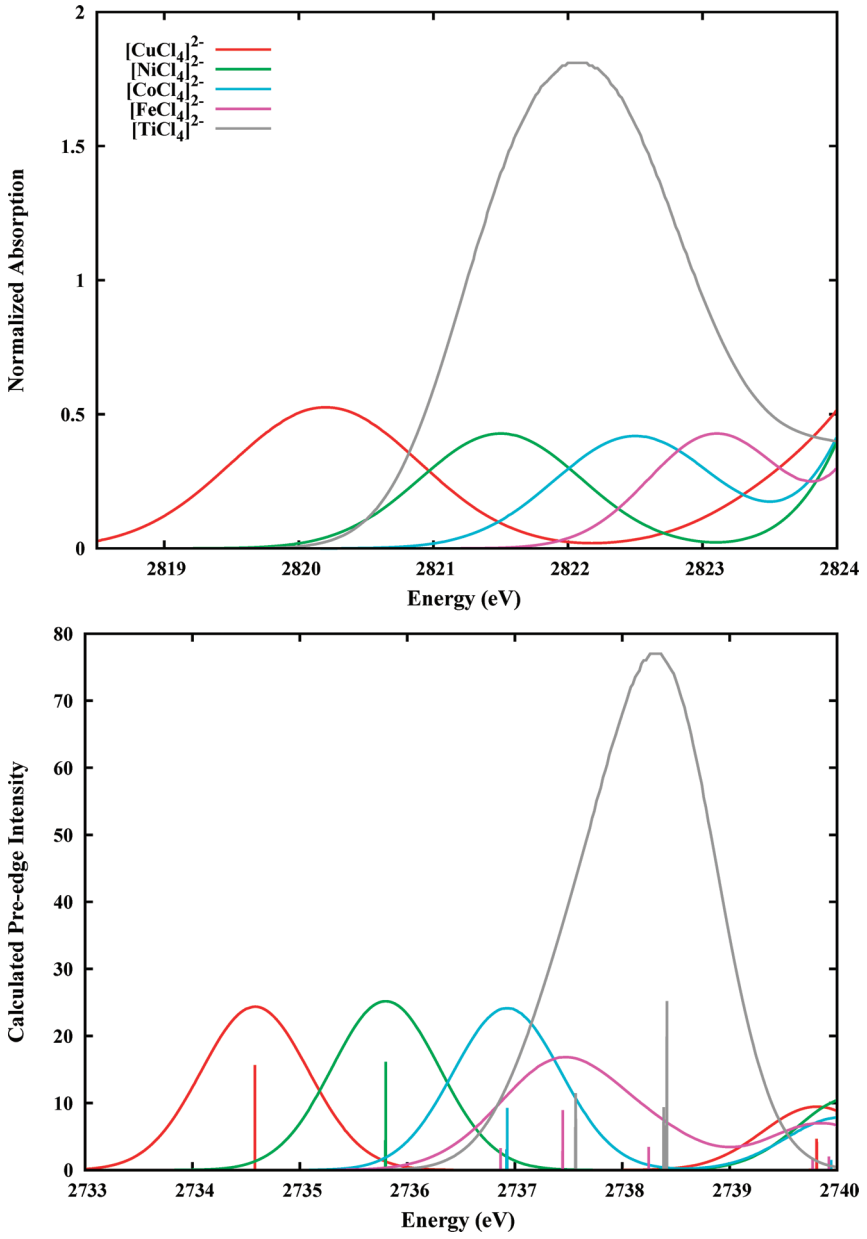

Figure 3. Comparison of experimental (top) Cl K-pre-edge XAS data to the calculated spectra (bottom). Experimental data are adapted from refs 67 and 68.

C. Cl K-Edge XAS Spectra for Metal Complexes. A series of metal tetrachlorides were constructed according to experimental X-ray structures,[59−62] and the Cl K-edge TDDFT XAS spectra were calculated with the BP86 functional[63,64] and TZVP basis set[65] following ref 35. XAS pre-edge features for five metal tetrachlorides ($[CuCl_4]^{2-}$, $[NiCl_4]^{2-}$, $[CoCl_4]^{2-}$, $[FeCl_4]^{2-}$, $[TiCl_4]^{0}$) were calculated using ES-TDDFT with initial guess transitions originating from core orbitals. An energy threshold of 2700 eV was utilized to target the top edge of core electron excitations, i.e,. a Cl 1s-core electron into a metal d-based MO.

For very high-energy transitions like X-ray absorptions that involve excitation of a core−electron, the spectroscopic oscillator strength needs to account for higher-order dipole interactions and takes on the form

$$f_I = f_I^{\mathrm{ed}} + f_I^{\mathrm{md}} + f_I^{\mathrm{eq}} \tag{20}$$

where $f_I^{ed} f_I^{md}$ and f_I^{eq} are electric dipole, magnetic dipole, and electric quadrupole oscillator strengths for the Ith transition, respectively. They are given by the following expressions in atomic units[35]

$$f_I^{\mathrm{ed}} = \frac{2}{3}\omega_I |\langle \Psi_0 | \hat{r} | \Psi_I \rangle|^2$$

$$f_I^{\mathrm{md}} = \frac{2}{3}\alpha^2 \omega_I |\langle \Psi_0 | \hat{l} + 2\hat{s} | \Psi_I \rangle|^2$$

$$f_I^{\mathrm{eq}} = \frac{1}{20}\alpha^2 \omega_I^3 \sum_{i,j} \left| \left\langle \Psi_0 \left| \hat{r}_i \hat{r}_j - \frac{1}{3} r^2 \delta_{ij} \right| \Psi_I \right\rangle \right|^2 \tag{21}$$

where α is the dimensionless fine-structure constant given as 1/137.03599 and ω_I is the excitation energy. Other notations

dx.doi.org/10.1021/ct200485x |J. Chem. Theory Comput. 2011, 7, 3540–3547

Table 3. Calculated Electric Dipole, Magnetic Dipole and Electric Quadrupole Oscillator Strength Contributions to Major Core−Electron Excitations Shown in Figure 3

metal complexes	excitation energy (eV)	electric dipole	magnetic dipole	electric quadruple
$[CuCl_4]^{2-}$	2734.58	$<10^{-3}$	$\sim 5 \times 10^{-3}$	15.67
	2739.75	0	0	0.21
	2739.81	$<10^{-3}$	0	4.66
$[NiCl_4]^{2-}$	2735.80	$<10^{-3}$	0	16.14
	2740.17	$<10^{-3}$	0	4.32
$[CoCl_4]^{2-}$	2736.93	$<10^{-3}$	0	9.23
	2739.94	$<10^{-3}$	0	1.51
	2740.08	$<10^{-3}$	0	2.55
$[FeCl_4]^{2-}$	2736.87	$<10^{-3}$	0	3.27
	2737.44	$<10^{-3}$	0	8.95
	2738.25	0	$\sim 10^{-3}$	3.46
	2739.77	$<10^{-3}$	0	1.70
	2739.92	$<10^{-3}$	0	2.01
$[TiCl_4]^{2-}$	2737.57	$\sim 10^{-3}$	$<10^{-3}$	11.99
	2738.39	$\sim 10^{-3}$	$\sim 10^{-3}$	9.80
	2738.42	$\sim 10^{-3}$	0	26.48

used are $\hat{r}$, the position operator; $\hat{l}$, the angular momentum operator; and $\hat{s}$, the spin operator.

Figure 3 shows a comparison of the experimental Cl K pre-edge data to the calculated pre-edge spectra where the oscillator strengths account for magnetic dipole and electric quadruple interactions in accordance with eqs 20 and 21. Oscillator strengths of electric dipole and electric quadrupole transitions are listed in Table 3. The calculated energies are underestimated (~85.6 eV on average), due to the limitations of DFT in modeling potentials near the nucleus, resulting in a Cl-1*s* orbital that is too high in energy relative to the valence orbitals.[35,66] The investigation of a systematic error in DFT such as this is beyond the scope of the present work. On the other hand, the calculated spectra are in good agreement with previously reported results from TDA type calculations.[35] The relative energies and intensities are also consistent with experimental observations.[67,68] The slight deviations from previous calculated spectra may arise from the use of an augmented basis set for the metal center and the dielectric continuum solvent that can lead to further stabilization of the valence orbitals.

IV. CONCLUSION

This paper presents an energy-specific TDHF/TDDFT method based on Davidson's iterative subspace algorithm. The method allows for the flexibility of only obtaining excitations above a predefined energy threshold enabling the prediction of an absorption spectrum over a specific energy range, such as extremely high-energy X-ray absorptions. Despite the fact that higher-energy transitions usually require a considerably large expansion vector space, this method shows an encouraging efficiency for large-scale systems. In about 30% of the time required for obtaining the full absorption spectra via the standard implementation of TDDFT, ES-TDDFT calculated the higher-energy ligand to metal charge transfer states for Mn^{2+}- and Co^{2+}-doped ZnO semiconducting nanocrystals. Most importantly, all of the calculated transitions are solved in the full MO space, ensuring that all of the excited states maintain orthogonality to the ground state and lower-lying excited states. Because the MO space is not restricted while solving for the transitions of interest, the calculated eigenvalues and eigenvectors are true solutions to the linear-response TDHF/TDDFT equations. As a result, characteristics of excited states obtained using the ES-TDHF/TDDFT method are essentially identical to those computed using the regular TDHF/TDDFT implementations.

AUTHOR INFORMATION

Corresponding Author
*E-mail: li@chem.washington.edu.

ACKNOWLEDGMENT

This work was supported by the U.S. National Science Foundation (CHE-CAREER 0844999 and CRC 0628252). Additional support from Gaussian Inc. and the University of Washington Student Technology Fund is gratefully acknowledged. Discussions with Ben Van Kuiken are greatly appreciated.

REFERENCES

(1) Foresman, J. B.; Head-Gordon, M.; Pople, J. A.; Frisch, M. J. *J. Phys. Chem.* **1992**, *96*, 135.
(2) Jorgensen, P.; Linderberg, J. *Int. J. Quantum Chem.* **1970**, *4*, 587.
(3) Olsen, J.; Jensen, H. J. A.; Jorgensen, P. *J. Comput. Phys.* **1988**, *74*, 265.
(4) Runge, E.; Gross, E. K. U. *Phys. Rev. Lett.* **1984**, *52*, 997.
(5) Gross, E. K. U.; Kohn, W. *Phys. Rev. Lett.* **1985**, *55*, 2850.
(6) Casida, M. E. *Recent Adv. Comput. Chem.* **1995**, *1*, 155.
(7) Casida, M. E.; Jamorski, C.; Casida, K. C.; Salahub, D. R. *J. Chem. Phys.* **1998**, *108*, 4439.
(8) Hirata, S.; Head-Gordon, M.; Bartlett, R. J. *J. Chem. Phys.* **1999**, *111*, 10774.
(9) Stratmann, R. E.; Scuseria, G. E.; Frisch, M. J. *J. Chem. Phys.* **1998**, *109*, 8218.
(10) Burke, K.; Werschnik, J.; Gross, E. K. U. *J. Chem. Phys.* **2005**, *123*, 062206.
(11) Dreuw, A.; Head-Gordon, M. *Chem. Rev.* **2005**, *105*, 4009.
(12) Nakatsuji, H. *Chem. Phys. Lett.* **1979**, *67*, 329.
(13) Koch, H. *J. Chem. Phys.* **1990**, *93*, 3345.
(14) Stanton, J. F.; Bartlett, R. J. *J. Chem. Phys.* **1993**, *98*, 7029.
(15) Krylov, A. I. *Annu. Rev. Phys. Chem.* **2008**, *59*, 433.
(16) Dallos, M.; Lischka, H.; Shepard, R.; Yarkony, D. R.; Szalay, P. G. *J. Chem. Phys.* **2004**, *120*, 7330.
(17) Kobayashi, Y.; Nakano, H.; Hirao, K. *Chem. Phys. Lett.* **2001**, *336*, 529.
(18) Finley, J.; Malmqvist, P.-A.; Roos, B. O.; Serrano-Andres, L. *Chem. Phys. Lett.* **1998**, *288*, 299.
(19) Iikura, H.; Tsuneda, T.; Yanai, T.; Hirao, K. *J. Chem. Phys.* **2001**, *115*, 3540.
(20) Heyd, J.; Scuseria, G. E.; Ernzerhof, M. *J. Chem. Phys.* **2003**, *118*, 8207.
(21) Tawada, Y.; Tsuneda, T.; Yanagisawa, S.; Yanai, T.; Hirao, K. *J. Chem. Phys.* **2004**, *120*, 8425.
(22) Rohrdanz, M. A.; Martins, K. M.; Herbert, J. M. *J. Chem. Phys.* **2009**, *130*, 054112.
(23) Dion, M.; Rydberg, H.; Schroeder, E.; Langreth, D. C.; Lundqvist, B. I. *Phys. Rev. Lett.* **2004**, *92*, 246401.
(24) Grimme, S. *J. Comput. Chem.* **2006**, *27*, 1787.
(25) Vydrov, O. A.; Van, V. T. *J. Chem. Phys.* **2010**, *133*, 244103.
(26) Maitra, N. T.; Zhang, F.; Cave, R. J.; Burke, K. *J. Chem. Phys.* **2004**, *120*, 5932.
(27) Casida, M. E. *J. Chem. Phys.* **2005**, *122*, 054111.

(28) Jacquemin, D.; Wathelet, V.; Perpete, E. A.; Adamo, C. *J. Chem. Theory Comput.* **2009**, *5*, 2420.
(29) Casarin, M.; Finetti, P.; Vittadini, A.; Wang, F.; Ziegler, T. *J. Phys. Chem. A* **2007**, *111*, 5270.
(30) Kozimor, S. A.; Yang, P.; Batista, E. R.; Boland, K. S.; Burns, C. J.; Christensen, C. N.; Clark, D. L.; Conradson, S. D.; Hay, P. J.; Lezama, J. S.; Martin, R. L.; Schwarz, D. E.; Wilkerson, M. P.; Wolfsberg, L. E. *Inorg. Chem.* **2008**, *47*, 5365.
(31) Besley, N. A.; Peach, M. J. G.; Tozer, D. J. *Phys. Chem. Chem. Phys.* **2009**, *11*, 10350.
(32) Stener, M.; Fronzoni, G.; de, S. M. *Chem. Phys. Lett.* **2003**, *373*, 115.
(33) Besley, N. A.; Noble, A. *J. Phys. Chem. C* **2007**, *111*, 3333.
(34) DeBeer, G. S.; Petrenko, T.; Neese, F. *J. Phys. Chem. A* **2008**, *112*, 12936.
(35) DeBeer, G. S.; Petrenko, T.; Neese, F. *Inorg. Chim. Acta* **2008**, *361*, 965.
(36) Tretiak, S.; Isborn, C. M.; Niklasson, A. M. N.; Challacombe, M. *J. Chem. Phys.* **2009**, *130*, 054111.
(37) Kauczor, J.; Jorgensen, P.; Norman, P. *J. Chem. Theory Comput.* **2011**, *7*, 1610.
(38) Niklasson, A. M. N.; Challacombe, M. *Phys. Rev. Lett.* **2004**, *92*, 193001.
(39) Coriani, S.; Hoest, S.; Jansik, B.; Thoegersen, L.; Olsen, J.; Jorgensen, P.; Reine, S.; Pawlowski, F.; Helgaker, T.; Salek, P. *J. Chem. Phys.* **2007**, *126*, 154108.
(40) Norman, P.; Bishop, D. M.; Jensen, H. J. A.; Oddershede, J. *J. Chem. Phys.* **2001**, *115*, 10323.
(41) Norman, P.; Bishop, D. M.; Jensen, H. J. A.; Oddershede, J. *J. Chem. Phys.* **2005**, *123*, 194103.
(42) Wilkinson, J. H. *The Algebraic Eigenvalue Problem*; Clarendon Press: Oxford, U. K., 1965; pp 582.
(43) Davidson, E. R. *J. Comput. Phys.* **1975**, *17*, 87.
(44) Hirao, K.; Nakatsuji, H. *J. Comput. Phys.* **1982**, *45*, 246.
(45) Bouman, T. D.; Hansen, A. E.; Voigt, B.; Rettrup, S. *Int. J. Quantum Chem.* **1983**, *23*, 595.
(46) MacDonald, J. K. L. *Phys. Rev.* **1933**, *43*, 830.
(47) Frisch, M. J.; Trucks, G. W.; Schlegel, H. B.; Scuseria, G. E.; Robb, M. A.; Cheeseman, J. R.; Scalmani, G.; Barone, V.; Mennucci, B.; Petersson, G. A.; Nakatsuji, H.; Caricato, M.; Li, X.; Hratchian, H. P.; Izmaylov, A. F.; Bloino, J.; Zheng, G.; Sonnenberg, J. L.; Liang, W.; Hada, M.; Ehara, M.; Toyota, K.; Fukuda, R.; Hasegawa, J.; Ishida, M.; Nakajima, T.; Honda, Y.; Kitao, O.; Nakai, H.; Vreven, T.; Montgomery, J. A., Jr.; Peralta, J. E.; Ogliaro, F.; Bearpark, M.; Heyd, J. J.; Brothers, E.; Kudin, K. N.; Staroverov, V. N.; Keith, T.; Kobayashi, R.; Normand, J.; Raghavachari, K.; Rendell, A.; Burant, J. C.; Iyengar, S. S.; Tomasi, J.; Cossi, M.; Rega, N.; Millam, J. M.; Klene, M.; Knox, J. E.; Cross, J. B.; Bakken, V.; Adamo, C.; Jaramillo, J.; Gomperts, R.; Stratmann, R. E.; Yazyev, O.; Austin, A. J.; Cammi, R.; Pomelli, C.; Ochterski, J. W.; Martin, R. L.; Morokuma, K.; Zakrzewski, V. G.; Voth, G. A.; Salvador, P.; Dannenberg, J. J.; Dapprich, S.; Parandekar, P. V.; Mayhall, N. J.; Daniels, A. D.; Farkas, O.; Foresman, J. B.; Ortiz, J. V.; Cioslowski, J.; Fox, D. J. *Gaussian Development Version H.12+*; Gaussian, Inc.: Wallingford, CT, 2011.
(48) Badaeva, E.; Feng, Y.; Gamelin, D. R.; Li, X. *New J. Phys.* **2008**, 10.
(49) Badaeva, E.; Isborn, C. M.; Feng, Y.; Ochsenbein, S. T.; Gamelin, D. R.; Li, X. *J. Phys. Chem. C* **2009**, *113*, 8710.
(50) Norberg, N. S.; Kittilstved, K. R.; Amonette, J. E.; Kukkadapu, R. K.; Schwartz, D. A.; Gamelin, D. R. *J. Am. Chem. Soc.* **2004**, *126*, 9387.
(51) Kittilstved, K. R.; Liu, W. K.; Gamelin, D. R. *Nat. Mater.* **2006**, *5*, 291.
(52) Liu, W. K.; Mackay, S. G.; Gamelin, D. R. *J. Phys. Chem. B* **2005**, *109*, 14486.
(53) Perdew, J. P.; Burke, K.; Ernzerhof, M. *Phys. Rev. Lett.* **1996**, *77*, 3865.
(54) Perdew, J. P.; Burke, K.; Ernzerhof, M. *Phys. Rev. Lett.* **1997**, *78*, 1396.
(55) Dunning, T. H., Jr.; Hay, P. J. *Mod. Theor. Chem.* **1977**, *3*, 1.
(56) Hay, P. J.; Wadt, W. R. *J. Chem. Phys.* **1985**, *82*, 299.
(57) Hay, P. J.; Wadt, W. R. *J. Chem. Phys.* **1985**, *82*, 270.
(58) Wadt, W. R.; Hay, P. J. *J. Chem. Phys.* **1985**, *82*, 284.
(59) Pauling, P. *Inorg. Chem.* **1966**, *5*, 1498.
(60) McGinnety, J. A. *J. Am. Chem. Soc.* **1972**, *94*, 8406.
(61) Lauher, J. W.; Ibers, J. A. *Inorg. Chem.* **1975**, *14*, 348.
(62) Dawson, A.; Parkin, A.; Parsons, S.; Pulham, C. R.; Young, A. L. C. *Acta Crystallogr., Sect. E: Struct. Rep. Online* **2002**, *E58*, i95.
(63) Becke, A. D. *Phys. Rev. A* **1988**, *38*, 3098.
(64) Perdew, J. P.; Burke, K.; Wang, Y. *Phys. Rev. B: Condens. Matter* **1996**, *54*, 16533.
(65) Schaefer, A.; Huber, C.; Ahlrichs, R. *J. Chem. Phys.* **1994**, *100*, 5829.
(66) Leeuwen, R. v.; Gritsenko, O. V.; Baerends, E. J. *Top. Curr. Chem.* **1996**, *180*, 107.
(67) Shadle, S. E.; Hedman, B.; Hodgson, K. O.; Solomon, E. I. *J. Am. Chem. Soc.* **1995**, *117*, 2259.
(68) DeBeer, G. S.; Brant, P.; Solomon, E. I. *J. Am. Chem. Soc.* **2005**, *127*, 667.